

Terrestrial Planet Finding with a Visible Light Coronagraph

Marc J. Kuchner¹

Harvard-Smithsonian Center for Astrophysics, Mail Stop 20, 60 Garden St., Cambridge, MA 02138

David N. Spergel

Princeton University Observatory, Peyton Hall, Princeton, NJ 08544

Abstract. Directly imaging extrasolar planets using a monolithic optical telescope avoids many pitfalls of space interferometry and opens up the prospect of visible light studies of extrasolar planetary systems. Future astronomical missions may require interferometry for high spatial resolution, but given that the first direct imaging missions will probably fit into a single launch vehicle, the astrophysics of planet finding calls for a visible light coronagraph as the first space mission to search for extrasolar terrestrial planets. New coronagraphic techniques place the necessary dynamic range within reach for detecting planets in reflected starlight.

1. Introduction

Bracewell's (1978) paper about using interferometry to separate the light from an extrasolar planet from the light of its host star spurred decades of research into interferometry as the canonical way to detect extrasolar terrestrial planets. Guided by NASA and ESA, a cohort of research groups around the world has been attacking the problems associated with interferometric planet finding: building achromatic nulling beam combiners and cryogenic coolers, operating formation flying spacecraft and automated fringe trackers, surveying exozodiacal dust backgrounds, etc. Laboratory tests suggest that a mid-infrared (mid-IR) interferometer with nulling beam combiners can generate the high dynamic range necessary for planet detection (Serabyn et al. 1999), and surely one day a mid-IR interferometer will obtain the accuracy required for extrasolar terrestrial planet finding.

But a monolithic optical telescope can also directly detect extrasolar planets. New coronagraphic techniques using masks and stops and deformable mirrors can potentially generate enough dynamic range to directly detect extrasolar terrestrial planets with a single optical telescope. We discuss astrophysical reasons for preferring a visible-light coronagraph for a first Terrestrial Planet Finder (TPF) and some of the new optical techniques that can power it.

¹Michelson Postdoctoral Fellow

2. Reasons for a Coronagraphic TPF

2.1. Inner Working Angle

TPF must find an extrasolar terrestrial planet and take its spectrum. No one knows how many stars must be searched to find such a planet, but clearly, more is better. A planet must have a minimum angular separation from its host star to be detectable by a given TPF design. This separation is the design’s “inner working angle”. The smaller the inner working angle of a TPF design, the more distant stars—and the more stars—it can search.

A coronagraph has an inner working angle between $2\lambda/D$ and $4\lambda/D$ (pushing this limit calls for more research). The primary mirror has longest dimension D , and visible light TPF operates at wavelengths $\lambda=0.4\text{--}1.1\ \mu\text{m}$. For example, a 4 m optical telescope would have an inner working angle of ~ 100 milliarcseconds ($4\lambda/D$ at $\lambda = 0.5\ \mu\text{m}$), or 1 AU at 10 pc. Conventional optical telescopes typically have circular primary mirrors, but since D is the longest dimension of the primary, elliptical mirrors are better for TPF. A coronagraph with a $6\text{ m} \times 2.7\text{ m}$ primary mirror, would be able to search roughly three times as many stars as the 4 m example, given the same collecting area.

A coronagraph offers a smaller inner working angle than an interferometer given the same size optics. A single-baseline nulling interferometer has an inner working angle of $\lambda/(4B)$, where B is the baseline and λ is roughly $8.5\text{--}15\ \mu\text{m}$. At first glance, it might seem that at a given inner working angle, $B \approx D$ within a factor of two. However, the single-baseline nuller generates a fringe pattern which varies as θ^2 at the null, where θ is the angle from the optical axis, so 10^{-4} of the light from a solar type star at 10 pc leaks through because of the finite size of the stellar disk. This leak would overwhelm the signal from an Earthlike planet, which would be $\sim 10^7$ times fainter than the star in the mid-IR. A visible-light coronagraph produces the equivalent of a θ^4 null (at least) and further separates starlight from the planet search area by imaging the star. Nulling interferometers must add additional long baselines to deepen the null, so that a 20 m mid-IR interferometer TPF and a 4 m diameter optical coronagraph TPF have comparable inner working angles.

2.2. Planet Characterization

After finding a planet, TPF must be able to characterize it—to monitor it and measure its spectrum to determine whether or not it is likely to be habitable. We would like to eventually have both mid-IR and visible wavelength ranges available to study extrasolar planet atmospheres. However, as a first measurement, a visible spectrum would provide compelling science, easily explained to taxpayers.

Studies of how to characterize extrasolar planets generally use the Earth as a reference point (Des Marais et al. 2001; Woolf et al. 2002). In the visible TPF band ($0.4\text{--}1.1\ \mu\text{m}$), we can measure the key biomarkers O_3 and O_2 on an Earth analog. We can also measure H_2O on an Earth analog, and other biologically important molecules CH_4 and CO_2 on an analog of the early Earth.

Rayleigh scattering dominates the short-wavelength end of the Earth’s visible spectrum, providing the blueness of the sky. Measuring this phenomenon on an extrasolar planet would indicate the total column depth of its atmosphere.

Visible light spectroscopy of the Earth also detects a tantalizing signature from vegetation, slightly too faint to detect on a true Earth twin, the “red edge” at $0.7\ \mu\text{m}$ (Seager & Ford 2003). TPF may not find little green men—but visible light TPF could find big red plants! Cloud patterns on the Earth have much higher contrast in the visible, and they remain stable long enough that a time series of visible photometry would indicate a planet’s rotational period (Ford et al. 2001).

Mid-IR spectroscopy of the Earth can also measure O_3 , H_2O , CO_2 , and if the wavelength range is extended shortward to $7\ \mu\text{m}$, possibly CH_4 . The mid-IR continuum also indicates a sort of mean temperature of the planet’s surface and cloud layers. The mid-IR offers no direct O_2 signature. The main mid-IR biomarker, the O_3 band at $9.7\ \mu\text{m}$, is a particularly strong feature and a sensitive indicator of small amounts of O_2 . But for the same reason, it is highly saturated in the Earth’s spectrum, making it a poor guide to the amount of atmospheric oxygen on an analog of today’s Earth.

2.3. Exozodiacal Dust

The brightest circumstellar source in the habitable zone of our solar system is not a planet but a disk of zodiacal dust, amounting to the equivalent of a single $\sim 50\ \text{km}$ asteroid crushed into $1\text{--}100\ \mu\text{m}$ grains. Other main sequence stars host similar “exozodiacal” clouds with up to $\sim 10,000$ times the surface brightness. An IDL routine to compute the surface brightness of exozodiacal clouds analogous to the solar zodiacal cloud is publicly available at <http://cfa-www.harvard.edu/~mkuchner/>.

An interferometric TPF acts like an antenna; it sums up the energy collected over a broad swath of the sky, modulated by a fringe pattern. A mid-IR interferometer with a baseline of less than a hundred meters can use a chopping scheme involving three or more dishes to subtract the background emission from a smooth exozodiacal cloud. However such a scheme can not subtract the photon noise in the solar zodiacal cloud or exozodiacal clouds. This constraint drives interferometric TPF designs toward using large 3 and 4 m diameter mirrors. An optical telescope, on the other hand, forms images, directing most of the light from an exozodiacal cloud onto a different detector pixel than the planet signal.

To complicate matters, known circumstellar clouds around other main sequence stars are not smooth; they contain knots of emission, which to a mid-IR TPF would resemble planets. Taking a spectrum of a blob of mid-IR emission—at a cost of perhaps weeks of integration time—can distinguish dust clump false alarms from planets. These blobs may arise from the dynamical perturbations of planets embedded in the dust. To some degree, we can also decode images of dust structures to infer the mass, orbital semi-major axis, and eccentricity of a perturbing planet (Kuchner & Holman 2003), and SIM should eventually be able to warn us about perturbing planets, possibly down to 3 Earth masses. But exozodiacal dust will make interpreting mid-IR interferograms of planetary systems more difficult and ambiguous.

At a given inner working angle, the angular resolution of a visible light coronagraph TPF ($2\text{--}4\ \lambda/D$ for an image mask, $3\text{--}4\ \lambda/D$ for a pupil mask) is a few times finer than the angular resolution of a mid-IR interferometer TPF ($\sim \lambda/L$ for a typical 3 or 4 dish system, where L is the total length of the structure).

This additional resolution allows a coronagraphic TPF to resolve structure in an exozodiacal cloud that would confuse a similarly-priced interferometric TPF. The linear resolution of a coronagraphic TPF is a factor of 2–4 higher than the linear resolution of an interferometer TPF at a given inner working angle; the improvement in exozodiacal background rejection goes as roughly the square of this number.

3. Very High Dynamic Range Optics

The Earth is $\sim 2 \times 10^{-10}$ as bright as the sun at visible wavelengths, where it shines in reflected sunlight. Before we can enjoy the advantages of working in the visible, we must show that coronagraphs can suppress the light from a planet’s host star to near this contrast level—three orders of magnitude more contrast than mid-IR TPF requires. The sources of background light that limit the contrast of a coronagraph divide into two categories: diffracted light from pupil and mask edges, and scattered light from imperfections in the optical surfaces.

3.1. Diffracted Light

In an ideal conventional optical telescope, such a faint source near a bright star would be overcome first by the sidelobes of the point spread function—Airy rings in the case of a circular aperture. If we ignore flaws in the optical surfaces, managing these sidelobes amounts to controlling how the telescope diffracts light.

The “diffracted light problem” permits an infinite family of solutions; this “problem” has been solved several times over. These solutions generally resemble interferometers mathematically. A coronagraph using a pupil-plane mask can be pictured as recreating the (u, v) coverage of a conventional interferometer with a carefully tapered beam, with greatly reduced sidelobes (Spergel 2001, Kasdin et al. 2003, Guyon 2003). A coronagraph using an image-plane mask recreates the fringe pattern of a nulling interferometer (Kuchner & Traub 2002), reducing both the sidelobes and the central peak of the stellar image. Both techniques offer a variety of options for handling the necessary compromise between search area, inner working angle, and throughput. The two techniques can work together in concert, though this possibility requires further exploration.

Coronagraphic masks draw on the class of “band-limited” functions and their Fourier transforms. The image mask transmissivity should be a band-limited function; the pupil mask transmissivity must be the Fourier transform of a band-limited function. A band-limited function has power only at low spatial frequencies. For example, a telescope has a finite diameter, D , so a pupil mask can not use baselines larger than D . Likewise, a band-limited image mask cannot use spatial frequencies higher than some fraction of D —the fraction of the pupil diameter blocked by the Lyot stop.

The trick is to design an efficient system that is robust to errors in manufacturing and control. The image-plane and pupil-plane masks described above can both be realized as binary masks, masks whose transmissivities are either 0 or 1. Binary masks can be created simply by cutting holes in opaque material, to a tolerance of roughly 1/3000 of the diffraction scale. Binary pupil masks can be manufactured to this specification at a cost of $< \$10,000$. For binary image

masks (Kuchner & Spergel 2003), the tolerance amounts to roughly 20 nm. This tolerance is routine for e-beam nano-lithography, though such an image mask has not yet been constructed.

Controlling diffracted light using image masks rather than pupil masks can provide somewhat better efficiency, particularly in terms of search time, but an image-plane coronagraph is substantially less tolerant than a pupil plane coronagraph to large-scale wavefront errors, such as pointing. The pointing requirements for an image-plane coronagraph are identical to the pointing requirements for a nulling interferometer with a quartic null given the same inner working angle; the distribution of pointing errors can have standard deviation up to $\sigma = 1.5$ mas for a 4 m coronagraph. A coronagraphic TPF could provide a choice of different kinds of both pupil and image masks on a pair of filter wheels.

3.2. Scattered Light

Any telescope has figure and reflectivity errors in its optical surfaces which scatter starlight into a background of speckles throughout the image-plane, coronagraphic masks notwithstanding. A TPF coronagraph would manage these speckles using active optics. The TPF system must be stable enough that the corrections need only be adjusted once every few hours, since it would take more than an hour of integration time to acquire enough photons to measure the speckles and decide how to update the correction.

Brown and Burrows (1990) referred to the ratio of the peak of the expected planet image to the typical scattered light background by the letter Q . Some designs call for operating at $Q \ll 1$ under the assumption that the speckle noise that will dominate their data can be averaged out. We believe that a TPF design should operate at $Q \geq 1$ to avoid the danger of systematic errors in the data and wavefront control which cannot be averaged away.

Of course, the speckle need only be controlled over the planet search area: angles $\sim 3\lambda/D$ to $\sim 60\lambda/D$ away from the image of the star. This search area corresponds to a range of spatial frequencies on the primary mirror. Achieving $Q \sim 1$ requires wavefront errors over these mid-spatial frequencies of < 0.5 Å rms in phase, and $< 10^{-3}$ rms in amplitude.

Figure 1 illustrates how a $Q \approx 1$ coronagraphic TPF image of a planet might appear. It shows the results of a broad band (0.66–1.0 μm) simulation of the performance of a 4 m coronagraph using a linear binary image mask (Kuchner & Spergel 2003) given 0.5 Å rms errors in wavefront phase and 10^{-3} rms errors in wavefront amplitude over the mid-spatial frequencies. The pointing error is assumed to be distributed in a Gaussian about zero with a standard deviation of 1.5 mas, and the image mask has errors in its shape at the level of 20 nm rms over spatial frequencies less than the diffraction scale. The grey curves show the images of a planet 2×10^{-10} times as bright as its host star and an exozodiacal cloud just like the solar zodiacal cloud at 5 pc assuming a 4m diameter primary. The top frame shows the attenuation of the planet light by the mask, and the bottom frame shows the surface brightness of the simulated images. PSF subtraction techniques like spectral deconvolution (Sparks & Ford 2002) could efficiently extract the planet signal from among the speckles.

Unlike the diffracted light problem, the scattered light problem will not be considered completely solved until a TPF coronagraph has successfully operated

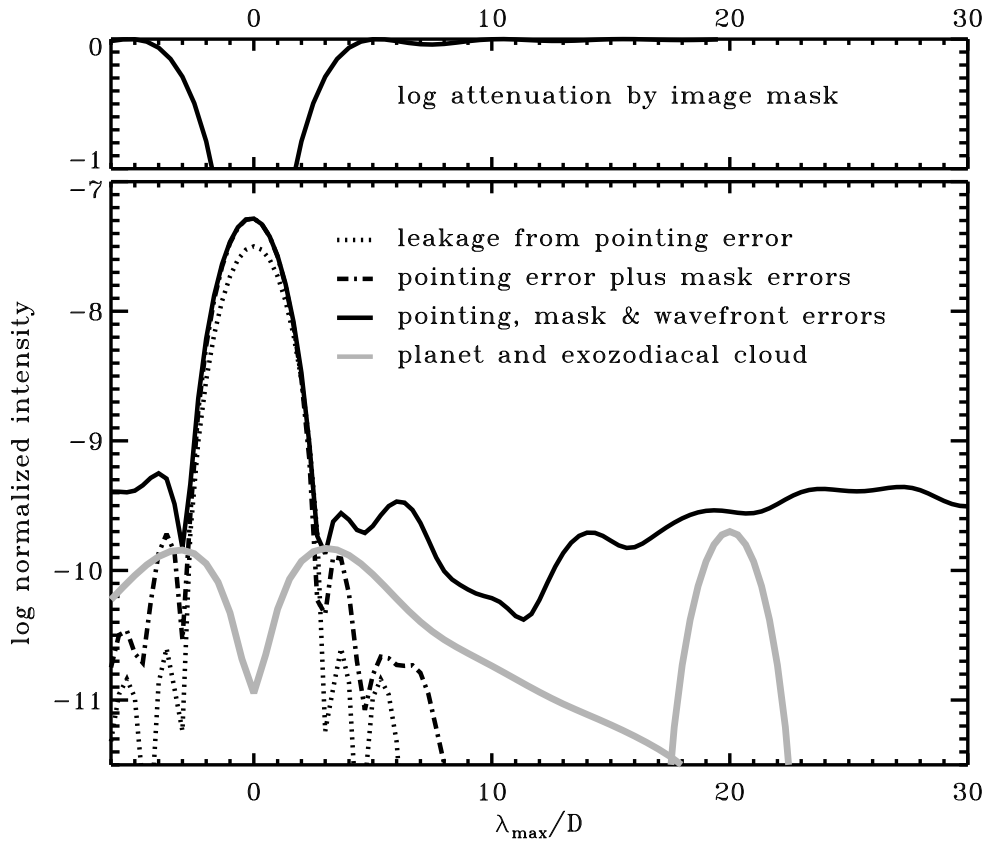


Figure 1. Broadband simulation of images produced by a coronagraphic TPF (Kuchner & Spergel 2003). The dotted curve shows leakage due to pointing error. The dot-dash curve adds errors to the shape of the binary image mask. The solid curve adds amplitude and phase errors to the incoming wavefront. The grey curves show images of a planet (at $20\lambda/D$) with relative flux 2×10^{-10} and a $1 \times$ solar exozodiacal cloud 5 pc distant assuming a 4m diameter primary. The upper panel shows the attenuation caused by the image mask.

in space. However, recent laboratory work suggests that this goal lies within reach. Experiments using a Xinetics deformable mirror at the High Contrast Imaging Testbed at JPL have demonstrated active mirror control to the 0.25 Å rms level (0.5 Å in wavefront phase) over mid-spatial frequencies (Trauger et al. 2002a). A pair of such mirrors can be combined to correct both phase and amplitude errors over a reasonable bandpass.

Space can provide the necessary highly stable environment. Thermal shields and other existing components appear to afford the necessary mechanical and thermal isolation given an L2 orbit and a mirror with a low thermal expansion coefficient, though some subtle structural effects—like micro-snap—remain unquantified. Other areas that demand investigation are the stability of optical coatings, and the sensitivity of the designs to polarization effects. These long-term stability concerns apply to mid-IR interferometers too; an interferometer TPF requires hours to form an image of a planet just as a coronagraphic TPF does, since the interferometer must rotate to fill out its (u, v) plane coverage.

Coronagraphy merits resources like those nulling interferometry has enjoyed for technology development and mission studies. The race for choosing a design for Terrestrial Planet Finder has led to a contest over which kind of high-dynamic range device is easier to manufacture and implement. Interferometry has a head start. But for a first mission to directly image planets, coronagraphy may have a shorter way to go.

4. Conclusion

A 10 m class space coronagraph (Beichman et al. 2002) could complete the originally mandated TPF survey of 150 F, G, and K stars. A smaller telescope (Brown et al. 2002)—perhaps one with an elliptical 6 by 2.7 m primary—probably suits the present TPF timeline. A 2 m class optical coronagraph in space (Trauger et al. 2002b) could directly image Jupiter analogs and extrasolar planets too far from their stars to detect by astrometric or precise-Doppler monitoring, and test the new technologies needed for directly imaging extrasolar terrestrial planets.

Both coronagraphy and interferometry require technological development before either technique can directly detect extrasolar terrestrial planets. Perhaps an affordable mid-IR nulling interferometer could also meet some of these scientific goals in the near future, and ultimately, follow-up missions to TPF will demand the angular resolution of a free-flying interferometer. These follow-up missions, however, might combine coronagraph and interferometer technologies. And in the meantime, coronagraphy may offer a better way to find and characterize and the first extrasolar analogs of Earth.

Acknowledgments. Thanks to Jeremy Kasdin, Steve Kilston, Charley Noecker and Wes Traub for close readings. This work was performed in part under contract with the Jet Propulsion Laboratory (JPL) through the Michelson Fellowship program funded by NASA as an element of the Planet Finder Program. JPL is managed for NASA by the California Institute of Technology.

References

- Beichman, C., Coulter, D., Lindensmith, C., & Lawson, P. eds. 2002, Summary Report on Architecture Studies for the Terrestrial Planet Finder (Pasadena: JPL Publication 02-011),
http://planetquest.jpl.nasa.gov/TPF/tpf_review.html
- Bracewell, R. N. 1978, *Nature*, 274, 780
- Brown, R. A. & Burrows, C. J. 1990, *Icarus*, 87, 484
- Brown, R. A., et al. 2002, *Proc. SPIE*, 4860
- Des Marais, D. J., Harwit, M., Jucks, K., Kasting, J. F., Lunine, J. I., Lin, D., Seager, S., Schneider, J., Traub, W., & Woolf, N. 2001, Biosignatures and Planetary Properties to be Investigated by the TPF Mission (Pasadena: JPL Publication 01-008),
http://planetquest.jpl.nasa.gov/TPF/tpf_review.html
- Ford, E., Seager, S. & Turner, E. L. 2001, *Nature*, 412, 885
- Guyon, O. 2003, *A&A*, in press, astro-ph/0301190
- Kasdin, N. J., Vanderbei, R. J., Spergel, D. N. & Littman, M. G. 2003, *ApJ*, 582, 1147
- Kuchner, M. J. & Holman, M. J. 2003, *ApJ*, in press, astro-ph/0209261
- Kuchner, M. J. & Spergel, D. N. 2003, *ApJ*, in press, astro-ph/0209271
- Kuchner, M. J. & Traub, W. A. 2002, *ApJ*, 570, 900
- Seager, S. & Ford, E. 2002, *Astrophysics of Life Conference Proceedings*, astro-ph/0212550
- Serabyn, E., Wallace, J. K., Hardy, G. J., Schmidtlin, E. G. H., & Nguyen, H. T. 1999, *Applied Optics*, 38, 7128
- Sparks, W. B. & Ford, H. C. 2002, *ApJ*, 578, 543
- Spergel, D. N. 2001, submitted to *Applied Optics*, astro-ph/0101142
- Trauger, J. et al. 2002a, *Proc SPIE*, 4860, "Performance of a Precision High-Density Deformable Mirror for Extremely High Contrast Astronomy from Space"
- Trauger, J. et al. 2002b, *Proc SPIE*, 4860, "The Eclipse Mission, a Direct Imaging Survey of Nearby Planetary Systems"
- Woolf, N. J., Smith, P. S., Traub, W. A. & Jucks, K. W. 2002, *ApJ*, 574, 430